# Analysis of the Control Effect and Influencing Factors of Urban Surface Deformation in Underground Coal Mining With Solid Backfilling

**Jiaqi Wang**
China university of mining and technology
**Zhang Qiang** ( leafkky@163.com )
China University of Mining and Technology
**Zhongya Wu**
China University of Mining and Technology
**Weijian Song**
China University of Mining and Technology
**Hao Zhang**
China University of Mining and Technology
**Yunbo Wang**
China University of Mining and Technology

**Research Article**

**Keywords:** urban surface deformation, coal mining, solid backfilling, monitoring, prediction parameters

**Posted Date:** March 22nd, 2021

**DOI:** https://doi.org/10.21203/rs.3.rs-221271/v1

# Abstract

To solve the problems of surface deformation and destruction of buildings caused by urban mining and realise coordinated development of mining cities, the solid backfilling method was used to extract coal resources beneath the buildings of Tangshan. Based on surface deformation monitoring data of the continuously operating reference station (CORS) system for the past 5 years, the surface deformation process caused by solid backfilling was analysed. The final results revealed a maximum surface subsidence of 66 mm in the T zone coal area and 31 mm in the F zone area. Furthermore, the surface control effects of the caving method and the solid backfilling method were compared and analysed, and it was shown that solid backfilling could meet the surface building set-up requirements. Moreover, based on the probability integral method, the effects on surface deformation due to the surface length of the F zone, compression ratio, and coal pillar width were analysed, and the effects on the prediction results due to the subsidence factor, tangent of the major effective angle, and offset distance of the inflection point were studied. The results showed that the compression ratio is the main factor controlling the surface deformation and that it should be kept above 80% for solid backfilling of urban mines. The subsidence factor should be 0.82 and the tangent of the major effective angle should be 2.15 when the surface subsidence of solid backfilling is to be predicted. This paper provides a technical reference for realisation of urban mining with solid backfilling.


# 1 Introduction

In recent years, the rapid development of China's economy has increased the demand for coal resources. In 2019 alone, China's coal production reached 3.85 billion tons, a year-on-year increase of 4% [1,2]. Such large-scale coal resource development has brought exhaustion of conventional coal resources, and some mines have had to explore coal resources beneath buildings, railways, and water bodies, which directly affects and restricts the harmonious development of ecology and society around the mining area. China's production of coal resources from beneath buildings, railways, and water bodies under unified allocation alone has reached 140 billion tons, with the amount of coal resources under buildings accounting for 70% of the total amount [3,4]. When such coal resources are mined, the surface deformation causes buildings to be stretched, compressed, and bent, thus causing various degrees of damage and collapse hazards to the buildings. Mining is also accompanied by the discharge of a large amount of solid waste gangue, which pollutes the environment and encroaches on the land. All of these problems cause serious conflicts in the development of a mining city.

The coal industry has been actively exploring ways to coordinate the development of coal mining and mining cities and has done considerable research and practical work. Solid backfill mining [5~7], which uses backfill to control rock movement and surface subsidence, has become the main technology to solve the conflicts between the development of the mine and the city. This technology has existed for some time and has been applied in more than 20 mines in China, effectively solving the problem of redundant resource extraction. However, long-term practice has shown that even the solid backfill mining method can cause large-scale movement and deformation of the ground surface. Current research on this problem has focused mainly on how the fill body controls rock movement, monitoring of surface movement and deformation, and analysis of disasters caused by surface deformation.

Many scholars have researched the aforementioned problems. Miao Xiexing [8~10], Zhang Jixiong [11-13], and Zhang Qiang [14,15] have advanced the equivalent mining height theory, key layer control theory, main roof control theory, and immediate roof control theory. These studies concluded that solid backfill mining can be regarded as extremely thin coal seam mining, allowing the surface subsidence to be controlled. The control targets for solid backfilling in the rock are the key layer, the main roof, and the immediate roof, with the first being the most difficult target and the last being the most precise target. Guo Guangli [16-18], Cha Jianfeng [19,20], Yao Qiangling [21,22] proposed the use of the probability

integral method to describe patterns of surface deformation, established a prediction model parameter system for surface subsidence with solid backfilling, and actually measured surface subsidence results using an electronic total station. Jiang Feifei [23] and Peng Fuhua [24] further analysed surface deformation characteristics using the analytic hierarchy process evaluation model and evaluation system.

The methods of surface deformation monitoring used in the aforementioned studies are not continuous and cannot show the surface deformation process caused by solid backfill mining because only the control effect of solid backfilling on the overlying rock layer was investigated. In this paper, taking the Tangshan mine as an example, 5 years of continuous surface subsidence data monitored by the continuously operating reference station (CORS) system were used to study the surface subsidence control effect of solid backfill mining. The effects on surface deformation due to surface length, compression ratio, and working surface arrangement were analysed. The effects of subsidence factor, tangent of major effective angle, and offset distance of the inflection point on the prediction results were also studied. Finally, the ranges of the compression ratio control index and the surface subsidence prediction parameters for solid backfill mining in urban mines were obtained.

# 2 Test Area

### 2.1 Mining geological conditions

Tangshan Mine, with a field area of 37.28 $km^2$ and a mining area of 55 $km^2$, is located in Lu'nan District, Tangshan City, Hebei Province. It is the only state-owned mega coal mine in China located in a city centre with convenient transportation access. Tangshan Mine uses the progressive mining area development method of inclined shafts. At present, there are 7 vertical shafts, which divide the mine into 10 production areas. There are no large-scale faults in the Tangshan mine field, and the main coal seams are the 5th, 8th, $9^{th}$, and 12th seams, with average thicknesses of 2.4, 3.7, 3.5, and 6.4 m, respectively. Among these, the 5th coal seam has an immediate roof consisting of 4.8 m thick fine sandstone and a bottom plate of 0.9 m thick mudstone, whereas the 9th coal seam has an immediate roof consisting of 0.7 m thick mudstone and a bottom plate of 1.0 m thick sandy mudstone. The geographical location of the Tangshan Mine is shown in Figure 1.

### 2.2 Mine and surface buildings

As shown in Figure 2, the production area of Tangshan Mine is located beneath the city. The main coal areas are the T zone and the F zone. The T zone has an area of 2.01 $km^2$ and 30.366 million tons of coal, of which 1.427 million tons have been mined to date. There are 67 community and office buildings on the surface. The F zone has an area of 1.27 $km^2$ and 34.413 million tons of coal, of which 34.26 million tons have been mined. Production and living facilities of the mine itself and a park exist at the surface. Figure 2 shows a comparison between the surface and subsurface structures.

### 2.3 Fortification and control indicators

Inspection results of the surface buildings show that the main structures of the surface buildings above Tangshan mine are brick–concrete, brick–wood, and steel structures, which meet the national requirements for Class II–III protection. When mining the coal resources beneath the city, the buildings must be kept below the Class I damage level after mining, i.e., horizontal deformation less than 2.0 mm/m, curvature less than 0.2 $mm/m^2$, and inclination less than 3.0 mm/m.

### 2.4 Solid backfilling control method

The solid backfill mining method, which is carried out through integrated mechanised mining operations on working faces, is used for mining under urban buildings. In the solid backfill coal mining system, the gangue is transported from the surface feeding well and underground separation chamber to the working faces, is then filled into the goaf using key equipment such as the multi-hole bottom dump conveyor and hydraulic support system for solid backfilling, and is finally compacted by the ramming mechanism behind the hydraulic support system. From 2015 to 2019, the surface feeding well accumulated 604,600 tons of gangue, and the underground separation system accumulated 421,100 tons of gangue. The backfilling system, shown in basic concept in Figure 3, is running well.

### 2.5 Mining on the working face

As examples, the $T_3$292 working face and the F5001 working face of the Tangshan Mine are shown schematically in Figure 4. The $T_3$292 working face has a length of 90 m, is elevated at an angle, and was in operation from 1 March 2013 to 1 April 2017. The F5001 working face has a length of 66 m, is also elevated at angle, and was in operation from 1 January 2016 to 1 September 2017.

## 3 Surface Deformation Monitoring Methods

### 3.1 Main existing monitoring methods

Monitoring the subsidence and deformation of the surface, buildings, and other structures is an important task in the process of mining beneath a city. The conventional monitoring methods used for the Tangshan Mine include mainly theodolite tracking, total station monitoring, and water level monitoring. The main problems faced in the monitoring process are addressed below. The accuracy of the conventional monitoring methods is not very high. Moreover, the detection process is easily affected by rain, snow, and the mutual obstruction of the surface buildings. In addition, the conventional monitoring systems are not capable of continuous monitoring.

### 3.2 Tangshan Mine monitoring method

The CORS system for intelligent monitoring of surface subsidence can carry out continuous and uninterrupted observation and achieve real-time collection, transmission, calculation, and analysis of data within the subsidence range. The CORS system applied in the Tangshan Mine is equipped with China's Beidou Satellite Navigation System, which is compatible with the United States' GPS system and Russia's GLONASS system, to improve the accuracy of surface subsidence deformation measurement. The CORS system basically consists of a data centre, a reference station, a data communication subsystem, and a user application subsystem. It achieves all-weather, fully automatic, and precise positioning through satellite positioning technology, the reference station, and the Internet. The CORS base station and Class I and II measuring points of the Tangshan Mine are shown in Figure 5.

### 3.3 Station layout

The $T_3$292 working face has two surface observation lines, i.e., line A and line L (Figure 6), with 22 points on line A and 8 points on line L. The F5001 working face has one surface observation line, line F, with a total of 22 points. The F5002 working face has four surface observation lines, lines N, S, W, and E.

## 4 Analysis Of Monitoring Results

The test used the surface subsidence monitoring data obtained from 1 January 2015 to 1 December 2019 as a reference to analyse the surface subsidence after mining on the $T_3$292 working face, F5001 working face, and F5002

working face. The monitoring data span more than 5 years and so can reflect the long-term surface deformation after solid backfill mining.

### 4.1 Surface monitoring results in Area T

The $T_3$292 working face was put into production in March 2013 and stopped being used in April 2017. Line A, measuring surface subsidence in the T zone, crosses the middle of the $T_3$292 working face, and the projected positions of the selected measuring points below the working face are located at a distance of 340 m from the open-off cut of the working face. The surface subsidence data of each measuring point on line A were obtained by processing the monitoring data, as shown in Figure 7(a). The surface subsidence data of each time period at the A9 measuring point are shown in Figure 7(b).

As shown in Figure 7(b), the surface subsidence increased slowly from the start of mining on the working face to June 2015, with the subsidence value lower than 25 mm. Between June 2017 and August 2017, after the working face was pushed 90 m beyond measuring point A9, the surface subsidence value increased significantly, with its maximum value reaching 41 mm at measuring point F16. In April 2017, the working face had been mined completely. By December 2019, the $T_3$292 working face had reached full mining impact and its maximum subsidence had increased to 66 mm. From the time of sudden subsidence to full mining impact, the subsidence value increased by approximately 37.8%.

The CORS monitoring system indicated a final maximum surface tilt deformation of 0.76 mm/m, a maximum curvature deformation of 0.064 mm/m$^2$, and a maximum horizontal deformation of 50.6 mm, or 1.53 mm/m, which meet the surface building protection requirements.

### 4.2 Surface monitoring results in F zone

(1) F5001 working face

The F5001 working face was put into production in October 2016 and stopped being used in September 2017. The line F, measuring surface subsidence in the F zone, crosses the middle of the F5001 working face, and the projected positions of the selected measuring points under the working face are located at 400 m from open-off cut of the working face. The monitoring data were processed to obtain the surface subsidence data of each measuring point on line F, as shown in Figure 8(a). The surface subsidence data of each time period of measuring point F9 are shown in Figure 8(b).

As shown in Figure 8(b), the surface subsidence increased slowly, with subsidence values lower than 10 mm, from the start of the mining on the working face to May 2017. Between June 2017 and July 2017, after the working face had pushed through 66 m from measuring point F9, the surface subsidence increased significantly, with a maximum value of 19 mm at measuring point F16. In November 2017, the working face was mined completely, and by April 2018, the F5001 working face had reached full mining impact and its maximum subsidence had increased to 31 mm. From sudden subsidence to full mining impact, the time elapsed was approximately 8 months and the subsidence value had increased by approximately 38.7%.

The CORS monitoring system indicated a final maximum surface tilt deformation of 1.65 mm/m, a maximum curvature deformation of 0.094 mm/m$^2$, and a maximum horizontal deformation of 16.1 mm, or 1.25 mm/m, which meet the surface building protection requirements.

(2) F5002 working face

The F5002 working face was put into production in November 2017 and stopped being used in December 2018. The line E, measuring surface subsidence in the F zone, crosses the middle of the F5002 working face, and the projected positions of the selected measuring points below the working face are located at 400 m from the open-off cut of the working face. The monitoring data were processed to obtain the surface subsidence data of each measuring point on line E, as shown in Figure 9(a). The surface subsidence data of each time period of measuring point E3 are shown in Figure 9(b).

As shown in Figure 9(b), there was almost no increase in surface subsidence from the start of mining on the working face to September 2018. Mining on the working face was fully stopped in December 2018, and by July 2019, the surface subsidence of the F5002 working face had reached 17 mm. By December 2019, the full mining impact had been reached, and the maximum increase in subsidence was 25 mm. From sudden subsidence to full mining impact, the time elapsed was approximately 5 months and there was an increase in subsidence value of approximately 47.1%.

The CORS monitoring system indicated a final maximum surface tilt deformation of 0.29 mm/m, a maximum curvature deformation of 0.012 mm/m$^2$, and a maximum horizontal deformation of 7.84 mm, or 0.81 mm/m, which meet the surface building protection requirements.

### 4.3 Comparison of control effects

Observation of the surface movement and deformation caused by mining on the F5009 working face started in February 2018, and a total of 27 observations were made until August 2020. Line n, measuring the surface subsidence in the caving area, crosses the middle of the F5009 working face, and the projected positions of the selected measurement points below the working face are located 400 m from the open-off cut of the working face. The surface subsidence data of each measurement point on line n are shown in Figure 10(a). The surface subsidence data of each time period of measuring point n4 are shown in Figure 10(b).

As shown in Figure 10(b), in comparison with solid backfill mining, the initial value of surface subsidence of the caving method was larger, reaching 60 mm. As mining on the working face continued, the value of surface subsidence increased gradually without any sudden increase. The maximum value of subsidence of measuring point n4 reached 210 mm by August 2020, when all of the mining operations on the working face had been completed.

The CORS monitoring system indicated a final maximum surface tilt deformation of 6.65 mm/m, a maximum curvature deformation of 0.59 mm/m$^2$, and a maximum horizontal deformation of 168.1 mm, or 4.25 mm/m, which do not meet the surface building protection requirements.

A comparison of surface deformation parameters between the solid backfill mining method and the caving method is shown in Table 1.

In addition, the relationship between surface subsidence values and monitoring time was analysed for $T_3$292, F5001, and F5002. The monitoring data were acquired at the time points of the goaf square period, end of mining, 3 months after mining, 1 year after mining, and 2 years after mining. The analysis results showed that the surface subsidence of backfill mining was significantly affected by monitoring time. Although the surface did not show large subsidence during the mining, surface subsidence increased significantly from 3 months to 1 year after mining. The time of 2 years after backfill mining can be regarded as the time when mining was completed, and the surface subsidence above the working face did not increase further at this time.

## 5 Results And Discussion

### 5.1 Analysis of factors influencing surface subsidence

Taking the F zone as an example, under the mining geological conditions of the Tangshan Mine, it is considered that the surface subsidence above the F zone was influenced by the face length, compression ratio of the working face, and width of the coal pillar in the section. To analyse the causes of surface subsidence, 15 sets of test plans were designed, as shown in Table 2. Tests 1–5 analysed the effect of face length on surface deformation parameters, tests 6–10 analysed the effect of compression ratio on surface deformation parameters, and tests 11–15 analysed the effect of coal pillar width on surface deformation parameters.

The surface deformation prediction uses the probability integral method based on equivalent mining height. Due to the presence of a large number of primary fissures, joints, and strata in the subsiding rock, it is feasible to predict surface movement and deformation by the probability integral method of random medium. Its main prediction parameters are shown in Table 3.

Predictions were made using an analysis software for coal mining subsidence prediction, and the results are shown in Table 4.

The surface subsidence, horizontal deformation, curvature, and tilt deformation under different influencing factors were analysed and compared. The test results obtained are shown in Figure 11.

As shown by the analysis in Figure 11, the subsidence, horizontal deformation, curvature, and tilt deformation increase gradually as the face length increases gradually. The subsidence, horizontal deformation, curvature, and tilt deformation decrease gradually as the compression ratio increases gradually, and the subsidence, horizontal deformation, curvature, and tilt deformation do not change much with increase in coal pillar width.

In particular, when the compression ratio is 0.3, i.e., the caving method is used to deal with the hollow area, the surface deformation exceeds the set damage level; thus, the compression ratio is the main influencing factor of surface deformation. From the predictive analysis of surface deformation, it is apparent that the compression ratio should be 0.6 or more to ensure the safety of surface buildings. In consideration of the influence due to early subsidence of the roof of the mining area, the compression ratio should be at least 0.8 in an actual backfilling operation.

### 5.2 Analysis of factors influencing the prediction results of surface subsidence

#### 5.2.1 Factors influencing the prediction parameters on the surface

In comparison with the caving method, when the probability integral method is used to predict surface subsidence for solid backfill mining, prediction parameters such as the subsidence factor, tangent of major effective angle, and offset distance of the inflection point change greatly. Therefore, these prediction parameters are considered to have a relatively large influence on the prediction results. Using a compression ratio of 0.8, 15 sets of test plans were designed to analyse the prediction results of surface deformation, and the plans are shown in Table 5. Tests 1–5 analysed the influence of the subsidence factor on the projected results, tests 6–10 analysed the influence of the tangent of the major effective angle on the prediction results, and tests 11–15 analysed the influence of the offset distance of the inflection point on the surface deformation parameters.

Predictions were made using an analysis software for coal mining subsidence prediction, and the results are shown in Table 6.

The surface subsidence, horizontal deformation, curvature, and tilt deformation under different influencing factors were analysed and compared. The test results obtained are shown in Figure 12.

From the analysis shown in Figure 12, as the subsidence factor increases gradually, the subsidence increases gradually while the horizontal deformation, curvature, and tilt deformation tend to stabilize. As the tangent of the major effective angle increases, the subsidence, horizontal deformation, curvature, and tilt deformation increase gradually. As the offset distance of the inflection point increases, the subsidence, horizontal deformation, curvature, and tilt deformation do not change.

It can be seen that the subsidence factor is the main influencing factor of the surface subsidence prediction results and that the tangent of the major effective angle is the main factor affecting the prediction results of surface horizontal deformation and tilt.

### 5.2.2 Calibration of predicted surface parameters for the Tangshan Mine

According to the surface subsidence monitoring results of the Tangshan Mine of previous years, the subsidence factor of the Tangshan Mine with the caving method was determined to be between 0.55 and 0.85, the tangent of the major effective angle was between 1.92 and 2.40, and the offset distance of the inflection point was 0. Through parameter inversion of the surface subsidence in the F zone, the subsidence factor of backfill mining was determined to be 0.028 and the tangent of the major effective angle was 1.20, as shown in Table 7.

As shown in Table 7, the surface subsidence prediction parameters currently obtained from monitoring one to two working faces are not accurate, as the subsidence factor is extremely low. The prediction with these parameters is thus not representative of the surface subsidence after mining in the area. Therefore, by comparing the predicted results of surface subsidence, considering multiple factors in the F zone, the subsidence factor appropriate for the predicted subsidence with solid backfill mining of underground coal in the Tangshan Mine was determined to be 0.82, and the tangent of the major effective angle is 2.15. At this time, the predicted result of surface subsidence is 152 mm, which can be regarded as the final amount of surface subsidence after the end of mining in the F zone.

## Conclusion

(1) The CORS system was used to monitor the surface subsidence of coal mining under Tangshan city, which spanned more than 5 years and covered the T zone and the F zone, corresponding to a mining area of 150,000 $m^2$. The monitoring results showed that the surface protection requirements of urban mining were met by solid backfill mining, which had gentler surface deformation than caving mining. The maximum subsidence in the T zone after 32 months of working face mining was 66 mm, and the maximum subsidence in the F zone after 6 months of working face mining was 31 mm.

(2) Through the multi-factor surface subsidence prediction based on the probability integral method, it was concluded that surface subsidence is strongly influenced by the working face length and the compression ratio. The surface deformation increases gradually as the face length increases and the compression ratio decreases. To ensure the safety of surface buildings, the compression ratio must be at least 0.8.

(3) By comparing the actual measurement data in the field with the quality simulation data, the subsidence factor suitable for the Tangshan Mine was finally determined to be 0.82 and the tangent of major effective angle was determined to be 2.15, at which time the predicted results are close to the subsidence results after extensive backfill mining in the mining area.

## Declarations

**Author Contributions:** All authors contributed equally to this research

**Funding:** All authors are grateful for the financial assistance provided by Independent Research Project of the State Key Laboratory of Coal Resources and Safe Mining, CUMT [SKLCRSM2020X01].

**Acknowledgments:** The authors thank the editorial board and the anonymous referees for their excellent comments, which greatly improved the paper.

**Conflicts of Interest:** The authors declare no conflicts of interest.

**The data used to support the findings of this study are included within the article.**

# References

1. Xie, H., Feng, G., Yang, J. U., & University, S. (2015) Research and development of rock mechanics in deep ground engineering. Chinese Journal of Rock Mechanics & Engineering, (11):2161-2178.
2. Xie, H. P., Gao, F., Ju, Y., Gao, M. Z., Zhang, R., & Gao, Y. N. (2015) Quantitative definition and investigation of deep mining. Journal of China Coal Society, 40(1), 1-10.
3. Xie, H. P., Zhou, H. W., Xue, D. J., Wang, H. W., Zhang, R., & Gao, F. (2012) Research and consideration on deep coal mining and critical mining depth. Journal of China Coal Society, 37(37), 535-542(8).
4. Yuan Liang (2016) Thoughts and suggestions on cracking major scientific and technological problems in deep coal mining. Science & Technology Review, (02):1.
5. Zhang, J. , Zhou, N. , Huang, Y. , & Zhang, Q. . (2011). Impact law of the bulk ratio of backfilling body to overlying strata movement in fully mechanized backfilling mining. Journal of Mining Science, 47(1), 73-84.
6. Qiang, Z. , Jixiong, Z. , Yanli, H. , & Feng, J. . (2012). Backfilling technology and strata behaviors in fully mechanized coal mining working face. International Journal of Mining Science and Technology, 22( 2), 151-157.
7. Zhang, J., Zhou, N., Huang, & Y., et al. (2011). Impact law of the bulk ratio of backfilling body to overlying strata movement in fully mechanized backfilling mining. JOURNAL OF MINING SCIENCE C/C OF FIZIKO-TEKHNICHESKIE PROBLEMY RAZRABOTKI POLEZNYKH ISKOPAEMYKH.
8. Zhou, D. , Wu, K. , Miao, X. , & Li, L. . (2018). Combined prediction model for mining subsidence in coal mining areas covered with thick alluvial soil layer. Bulletin of Engineering Geology and the Environment, 77(1), 283-304.
9. Zhang, J. , Zhang, Q. , Spearing, A. J. S. S. , Miao, X. , Guo, S. , & Sun, Q. . (2017). Green coal mining technique integrating mining-dressing-gas draining-backfilling-mining. International Journal of Mining Science & Technology, 27(1), 17-27.
10. Yin, W. , Miao, X. , Zhang, J. , & Zhong, S. . (2017). Mechanical analysis of effective pressure relief protection range of upper protective seam mining. International Journal of Mining Science and Technology.
11. Yan, H. , Zhang, J. , Zhou, N. , Zhang, S. , & Dong, X. . (2018). Shaft failure characteristics and the control effects of backfill body compression ratio at ultra-contiguous coal seams mining. Environmental Earth Sciences, 77(12), 458.
12. Zhang, J. , Sun, Q. , Fourie, A. , Ju, F. , & Dong, X. . (2018). Risk assessment and prevention of surface subsidence in deep multiple coal seam mining under dense above-ground buildings: case study. Human and Ecological Risk Assessment, 25(4), 1-15.
13. Hao, Y. , Jixiong, Z. , Sheng, Z. , & Nan, Z. . (2019). Physical modeling of the controlled shaft deformation law during the solid backfill mining of ultra-close coal seams. Bulletin of Engineering Geology and the Environment, 78, 3741–3754.
14. Qiang Sun, sup, Jixiong Zhang, Qiang Zhang, & HaoYan. (2018). A case study of mining induced impacts on the stability of multi-tunnels with the backfill mining method and controlling strategies. Environmental Earth

Sciences(77).

15. Qiang, Z. , Ji-Xiong, Z. , Wen-Yue, Q. I. , Nan, Z. , & Yang, T. . (2017). Structure optimal design research on backfill hydraulic support. Journal of Central South University (English Edition), 24(007), 1637-1646.
16. Li, H. , Zha, J. , Guo, G. , Zheng, N. , & Gong, Y. . (2020). Improvement of resource recovery rate for underground coal gasification through the gasifier size management. Journal of Cleaner Production, 259, 120911.
17. Liu, X. , Guo, G. , & Li, H. . (2020). Thermo-mechanical coupling numerical simulation method under high temperature heterogeneous rock and application in underground coal gasification. Energy Exploration & Exploitation(4), 014459871988898.
18. Zhang, G. , Lv, Y. , Guo, G. , & Yu, C. . (2020). Monitoring deep mining similarity material model of super-thick and weak cementation overburden by digital photography. IOP Conference Series Materials Science and Engineering, 782, 022028.
19. Qi-Chun, W. , Guang-Li, G. , Jian-Feng, Z. , & Yong, X. . (2013). Study on surface ground movement law of coal rejects backfill mining under thick and loose overburden strata. Coal Science and Technology.
20. Li, H. , Guo, G. , & Zheng, N. . (2018). Influence of coal types on overlying strata movement and deformation in underground coal gasification without shaft and prediction method of surface subsidence. Process Safety and Environmental Protection, 120, 302-312.
21. Yao, Q. L. , Xia, Z. , Tang, C. J. , Zhu, L. , & Tan, Y. M. . (2020). Characteristics of heavy metal ion adsorption by silty mudstones in coal mine goafs. Geofluids, 2020(4), 1-17.
22. Chong, Z. , Yao, Q. , Li, X. , & Shivakumar, K. . (2020). Acoustic emission investigation on scale effect and anisotropy of jointed rock mass by the discrete element method. Arabian Journal of Geosciences, 13(9), 1-14.
23. Feifei, J. , Xiangdong, L. I. , Bing, W. , & Qiang, L. I. . (2016). Influence analysis of strata movement in subsequent cemented filling of panel second-step stopes. Mining Research and Development.
24. Niu, D. X. , Wang, P. , Wang, Q. , Hua, F. Y. , Wang, F. , & Cai, Z. H. . (2014). Analysis of the power plant security management capability based on the ism and ahp. Advanced Materials Research, 960-961, 1477-1482.

# Tables

**Table 1 Comparison of surface deformation parameters between infill mining and collapse mining.**

| Mining method | Working face | Maximum subsidence (mm) | Maximum tilt deformation (mm/m) | Maximum curvature deformation ($mm/m^2$) | Maximum horizontal deformation value (mm) | Maximum horizontal deformation (mm/m) |
|---|---|---|---|---|---|---|
| Backfill method | T3292 | 66 | 0.76 | 0.064 | 50.6 | 1.53 |
| | F5001 | 31 | 1.65 | 0.094 | 16.1 | 1.25 |
| | F5002 | 25 | 0.29 | 0.012 | 7.84 | 0.81 |
| Caving method | F5009 | 210 | 6.65 | 0.59 | 168.1 | 4.25 |

**Table 2 Description of test plans.**

| Factor | Face length | Compression ratio | Coal pillar width | Factor | Face length | Compression ratio | Coal pillar width |
|---|---|---|---|---|---|---|---|
| Test 1 | 40 | 0.8 | 5 | Test 9 | 60 | 0.8 | 5 |
| Test 2 | 50 | 0.8 | 5 | Test 10 | 60 | 0.9 | 5 |
| Test 3 | 60 | 0.8 | 5 | Trial 11 | 60 | 0.8 | 0 |
| Test 4 | 70 | 0.8 | 5 | Trial 12 | 60 | 0.8 | 5 |
| Test 5 | 80 | 0.8 | 5 | Trial 13 | 60 | 0.8 | 10 |
| Test 6 | 60 | 0.3 | 5 | Trial 14 | 60 | 0.8 | 15 |
| Test 7 | 60 | 0.6 | 5 | Test 15 | 60 | 0.8 | 20 |
| Test 8 | 60 | 0.7 | 5 | | | | |

**Table 3 Table of prediction parameters for the working face.**

| Parameter | Azimuth (°) | Mining height (m) | Coal seam dip angle $\alpha$ | Subsidence factor $q$ | Tangent of major effective angle $tan\beta$ | Horizontal movement coefficient $b$ | Mining impact propagation angle $\theta$ |
|---|---|---|---|---|---|---|---|
| F5001 | 78 | 2.4 | 11 | 0.82 | 2.15 | 0.35 | 84.94 |
| F5002 | 78 | 2.4 | 13 | 0.82 | 2.15 | 0.35 | 84.02 |

**Table 4 Predicted results.**

| Test | Subsidence | Horizontal deformation | Curvature | Tilt | Test | Subsidence | Horizontal deformation | Curvature | Tilt |
|---|---|---|---|---|---|---|---|---|---|
| 1 | 108 | -0.7 | -0.01 | ±0.5 | 9 | 152 | -1.0 | -0.01 | ±0.7 |
| 2 | 131 | -0.9 | -0.01 | ±0.6 | 10 | 76 | -0.5 | 0 | 0.4 |
| 3 | 152 | -1.0 | -0.01 | ±0.7 | 11 | 153 | -1.0 | -0.01 | ±0.7 |
| 4 | 173 | -1.1 | 0 | ±0.8 | 12 | 152 | -1.0 | -0.01 | ±0.7 |
| 5 | 194 | -1.2 | -0.01 | 0.9 | 13 | 152 | -1.0 | -0.01 | ±0.7 |
| 6 | 533 | -3.4 | -0.03 | 2.5 | 14 | 151 | -1.0 | -0.01 | ±0.7 |
| 7 | 304 | -2.0 | -0.02 | 1.5 | 15 | 150 | -0.9 | -0.01 | ±0.7 |
| 8 | 228 | -1.5 | ±0.01 | 1.1 | | | | | |

**Table 5 Description of test plans.**

| Factor | Subsidence factor | Tangent of major effective angle | Offset distance of the inflection point | Factor | Subsidence factor | Tangent of major effective angle | Offset distance of the inflection point |
|---|---|---|---|---|---|---|---|
| Test 1 | 0.78 | 2.15 | 0.086 | Test 9 | 0.82 | 2.35 | 0.086 |
| Test 2 | 0.80 | 2.15 | 0.086 | Test 10 | 0.82 | 2.55 | 0.086 |
| Test 3 | 0.82 | 2.15 | 0.086 | Trial 11 | 0.82 | 2.15 | 0.006 |
| Test 4 | 0.84 | 2.15 | 0.086 | Trial 12 | 0.82 | 2.15 | 0.046 |
| Test 5 | 0.86 | 2.15 | 0.086 | Trial 13 | 0.82 | 2.15 | 0.086 |
| Test 6 | 0.82 | 1.75 | 0.086 | Trial 14 | 0.82 | 2.15 | 0.126 |
| Test 7 | 0.82 | 1.95 | 0.086 | Test 15 | 0.82 | 2.15 | 0.166 |
| Test 8 | 0.82 | 2.15 | 0.086 | | | | |

**Table 6 Predicted results.**

| Test | Subsidence | Horizontal deformation | Curvature | Tilt | Test | Subsidence | Horizontal deformation | Curvature | Tilt |
|---|---|---|---|---|---|---|---|---|---|
| 1 | 145 | -0.9 | -0.01 | ±0.7 | 9 | 167 | -1.2 | -0.01 | 0.9 |
| 2 | 148 | -1.0 | -0.01 | ±0.7 | 10 | 181 | -1.3 | ±0.01 | ±1.0 |
| 3 | 152 | -1.0 | -0.01 | ±0.7 | 11 | 152 | -1.0 | -0.01 | ±0.7 |
| 4 | 156 | -1.0 | -0.01 | ±0.7 | 12 | 152 | -1.0 | -0.01 | ±0.7 |
| 5 | 159 | -1.0 | -0.01 | 0.8 | 13 | 152 | -1.0 | -0.01 | ±0.7 |
| 6 | 121 | -0.6 | 0 | 0.5 | 14 | 152 | -1.0 | -0.01 | ±0.7 |
| 7 | 137 | -0.8 | -0.01 | ±0.6 | 15 | 152 | -1.0 | -0.01 | ±0.7 |
| 8 | 152 | -1.0 | -0.01 | ±0.7 | | | | | |

**Table 7 Calibration of projected surface parameters for the Tangshan mine.**

| Item | Subsidence factor | Tangent of major effective angle | Offset distance of the inflection point | Horizontal movement coefficient | Mining impact propagation angle |
|---|---|---|---|---|---|
| Caving method | 0.55~0.85 | 1.92~2.4 | 0 | 0.33 | 82 |
| Backfilling method (Experience) | 0.85~0.89 | 1.62~2.20 | 0.05~0.240 | 0.33 | 82 |
| Backfilling method<br><br>(Measured) | 0.028 | 1.20 | 0 | 0.33 | 82 |
| Backfilling method<br><br>(Simulated) | 0.82 | 2.15 | 0 | 0.33 | 82 |

## Figures

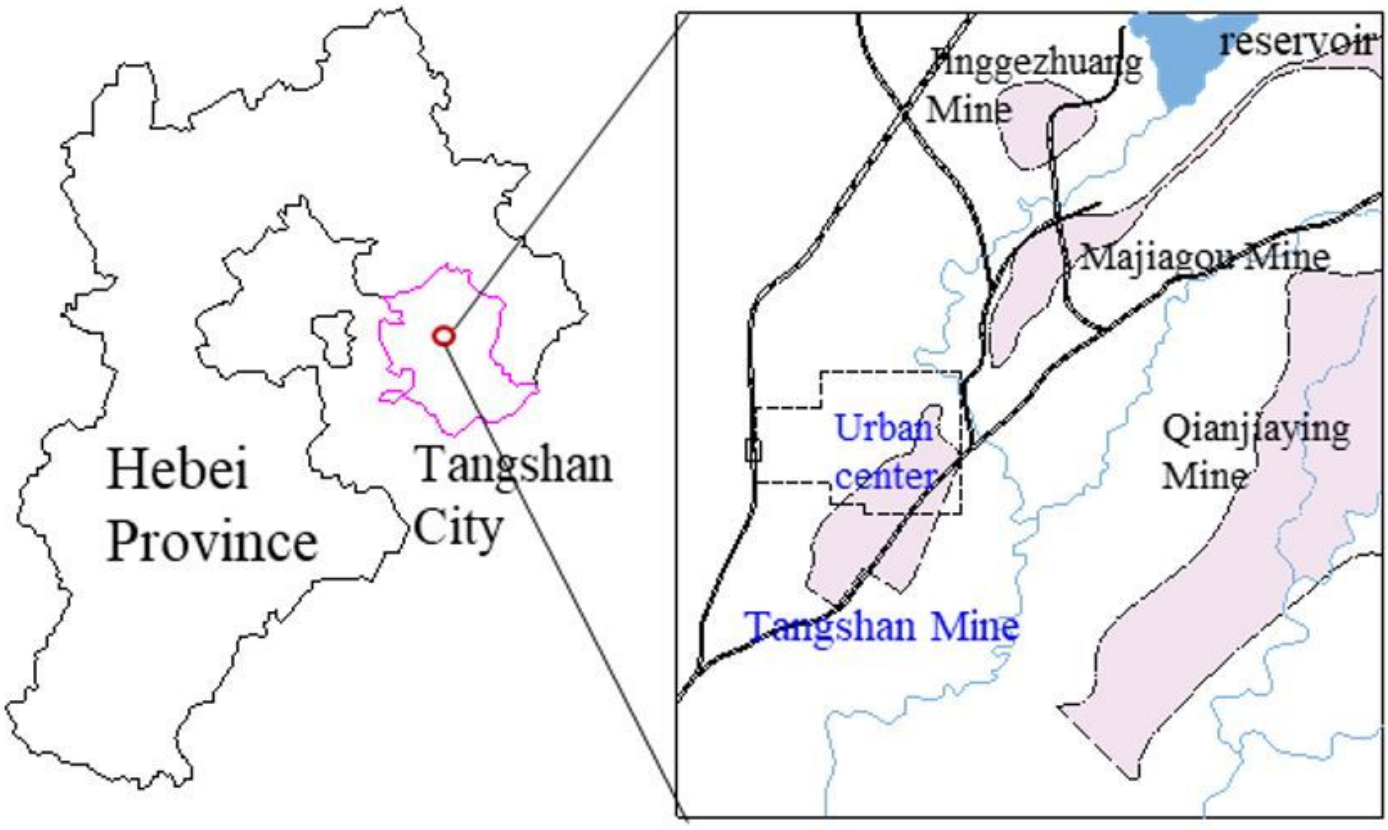


**Figure 1**

Geographical location and distribution of Tangshan mine. Note: The designations employed and the presentation of the material on this map do not imply the expression of any opinion whatsoever on the part of Research Square

concerning the legal status of any country, territory, city or area or of its authorities, or concerning the delimitation of its frontiers or boundaries. This map has been provided by the authors.


**Figure 2**

Tangshan mine surface–subsurface comparison.

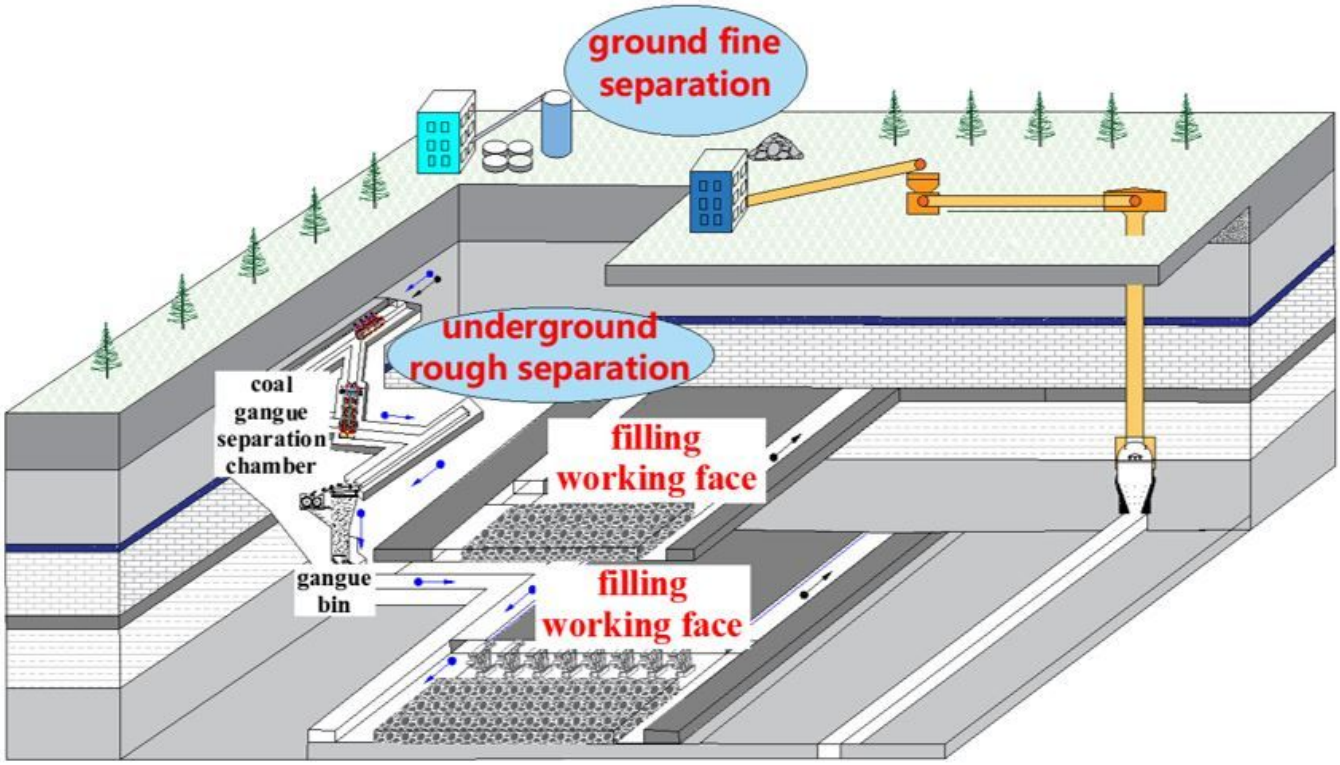


**Figure 3**

Basic concept of solid fill mining.

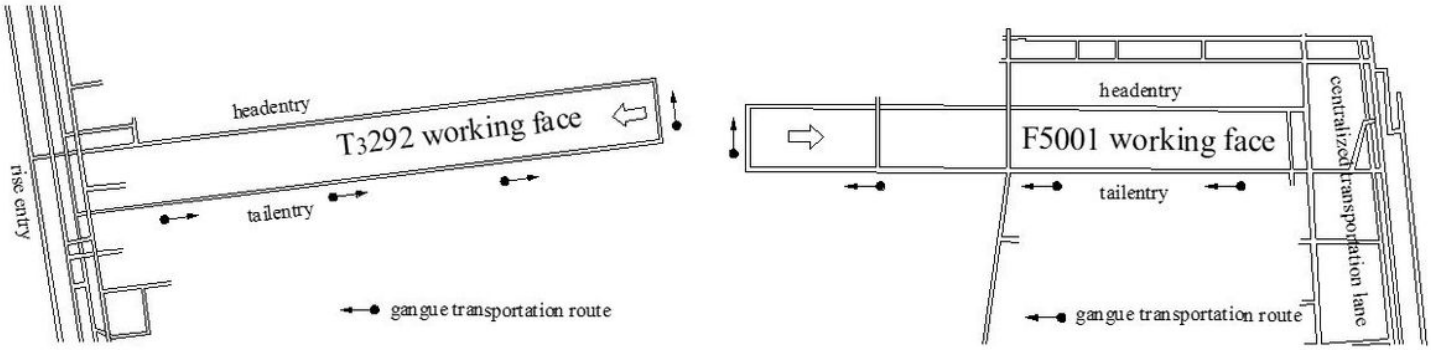


(a) Layout of $T_3292$ working face

(b) Layout of F5001 working face

**Figure 4**

Layout of working faces.

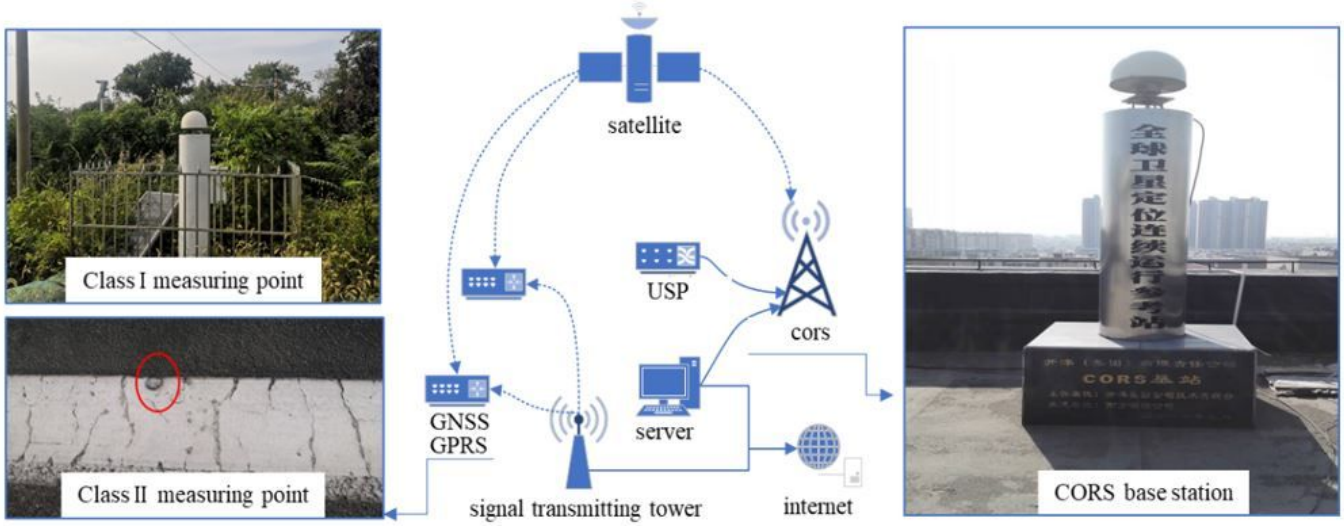


**Figure 5**

CORS base station and measuring points at Tangshan Mine.

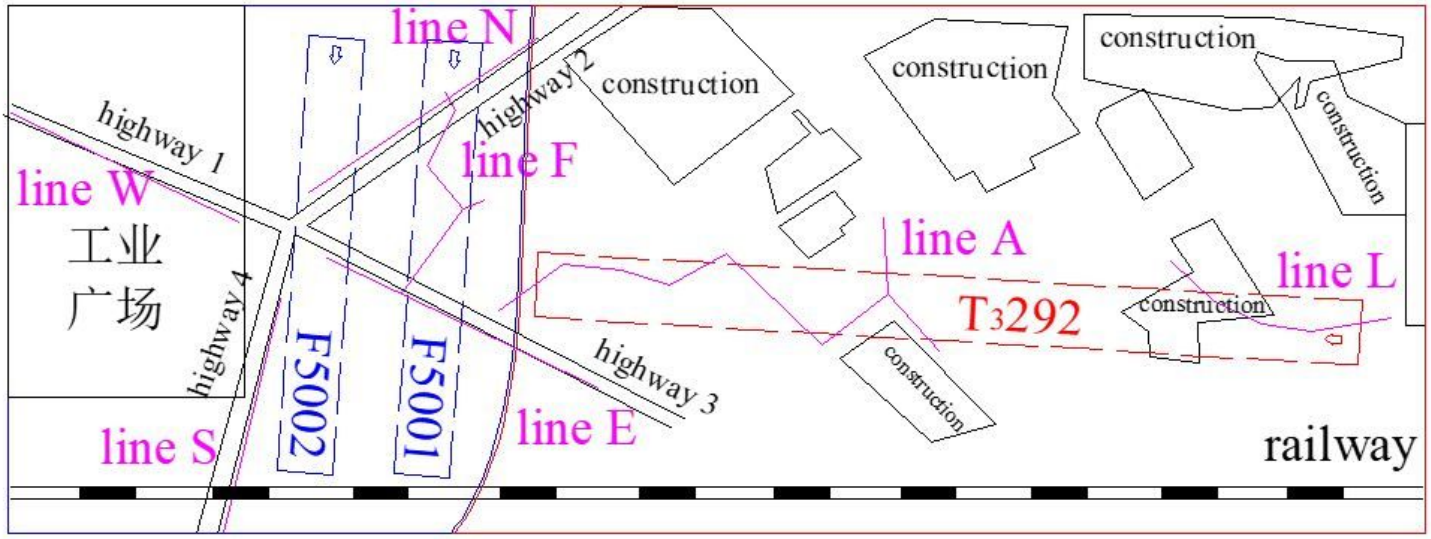


**Figure 6**

Arrangement of surface deformation observation points on solid backfill mining working faces.

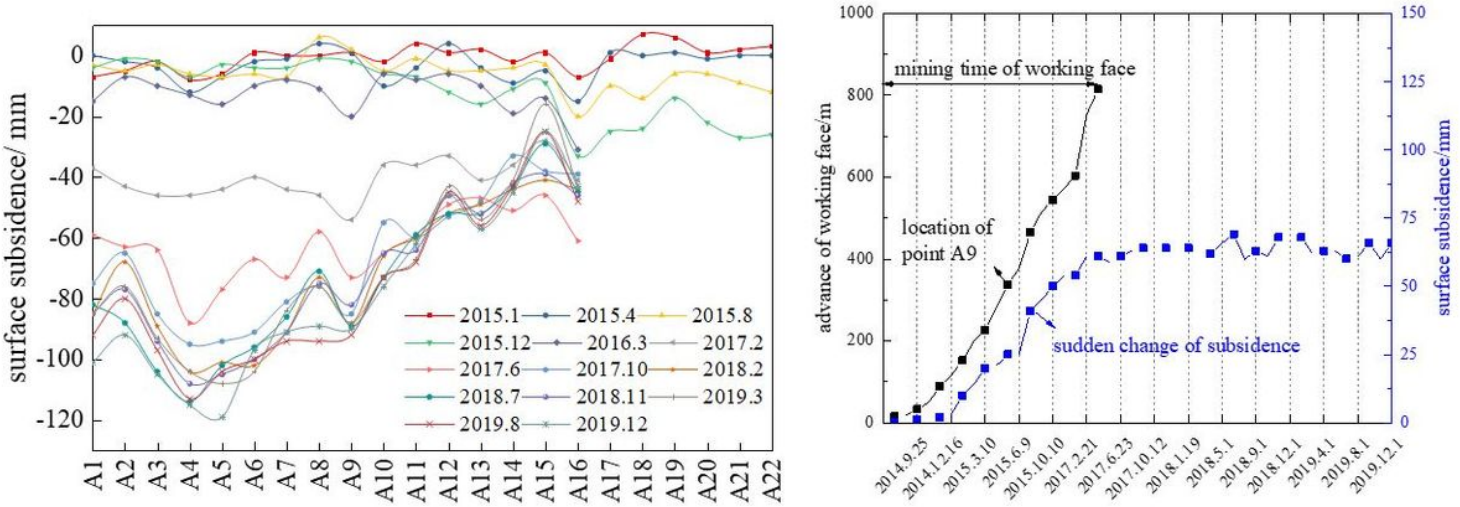


(a) Surface subsidence values on line A for each time period (b) Surface subsidence values for each time period at measuring point A9

**Figure 7**

Surface subsidence values.

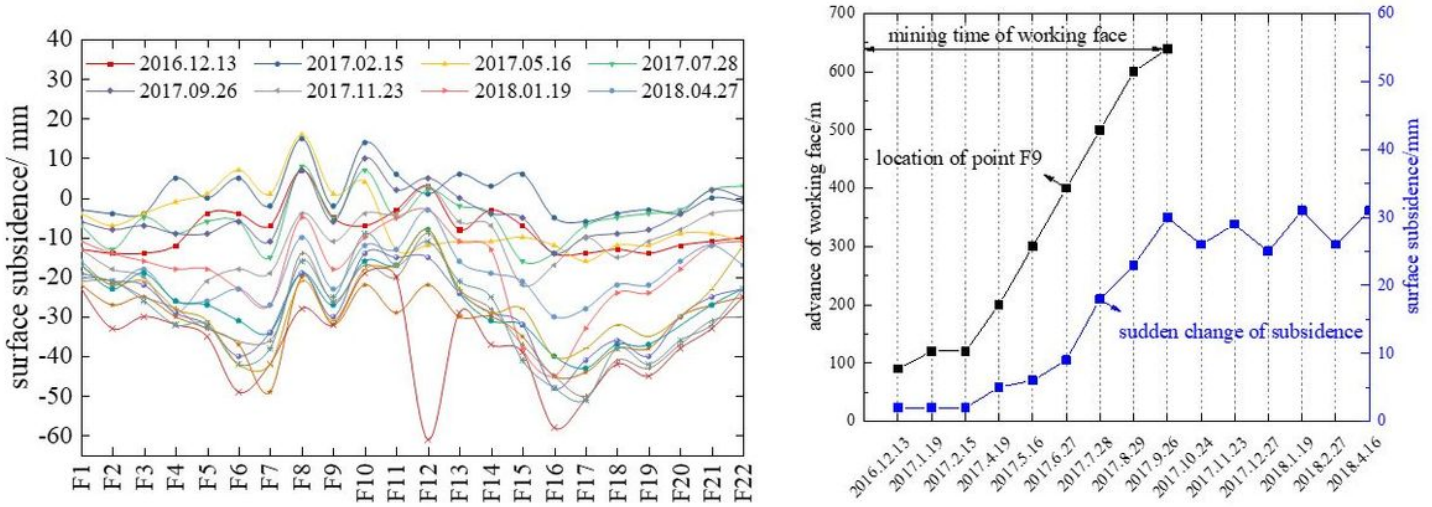


(a) Surface subsidence values on line F for each time period (b) Surface subsidence values for each time period at measuring point F9

**Figure 8**

Surface subsidence values.

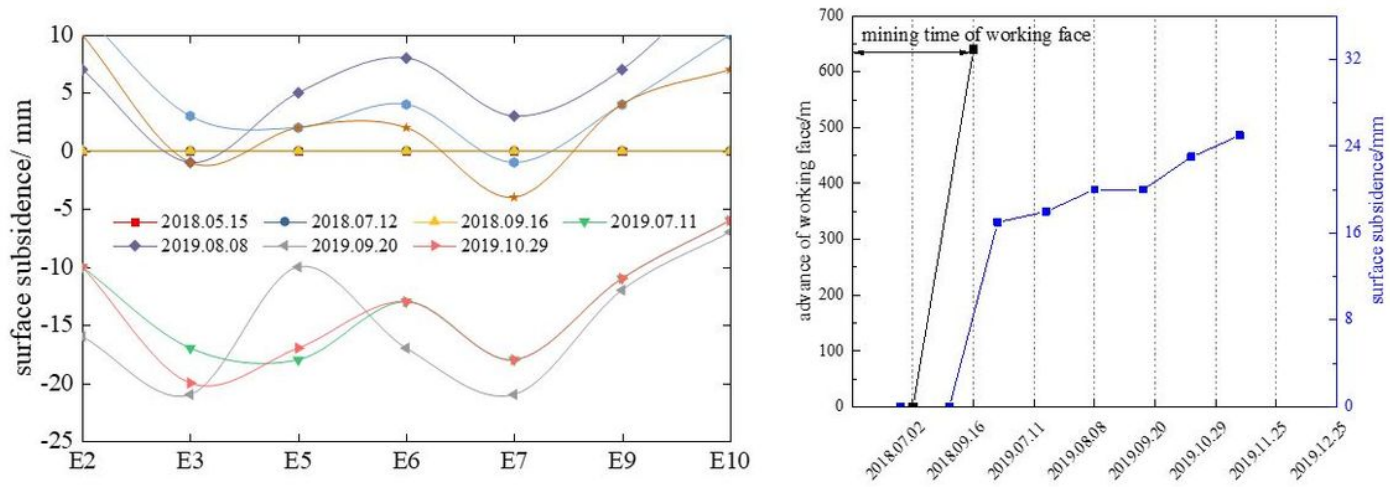


(a) Surface subsidence values at line E for each time period (b) Surface subsidence values for each time period at measuring point E3

**Figure 9**

Surface subsidence values.

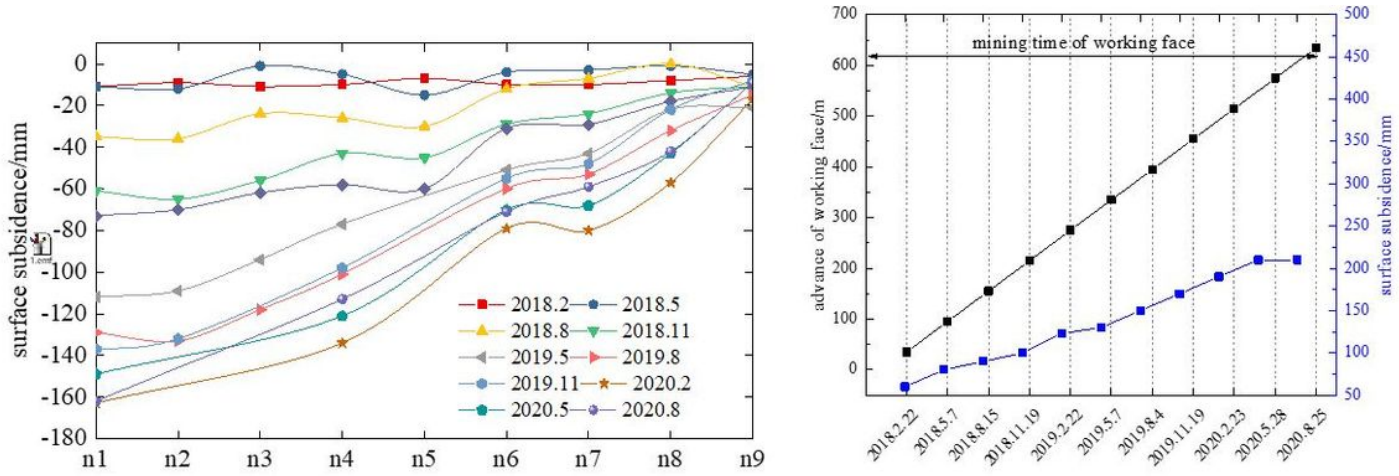


(a) Surface subsidence values on line n for each time period (b) Surface subsidence values for each time period at measuring point n4

**Figure 10**

Surface subsidence values.

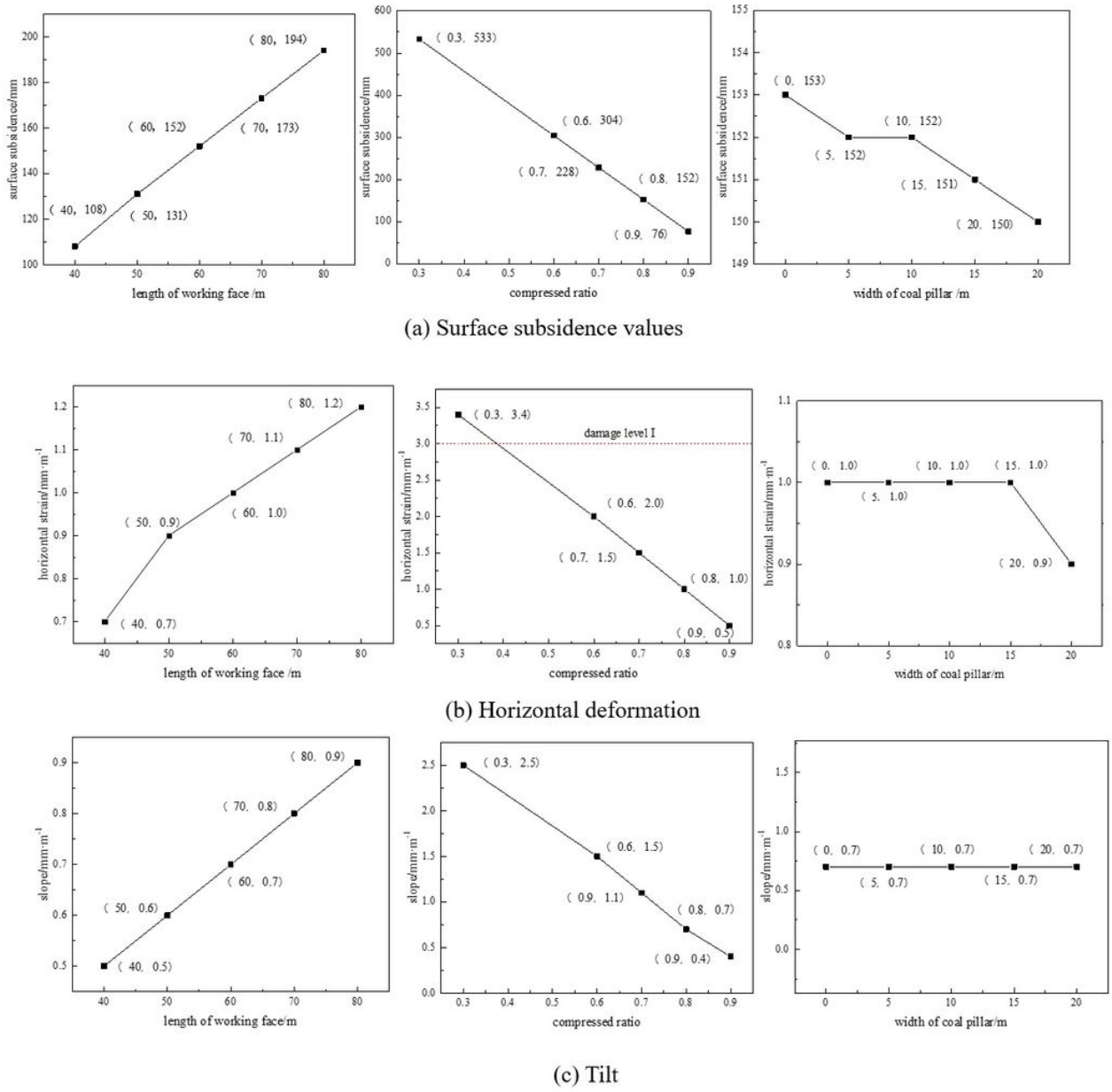


**Figure 11**

Experimental results.

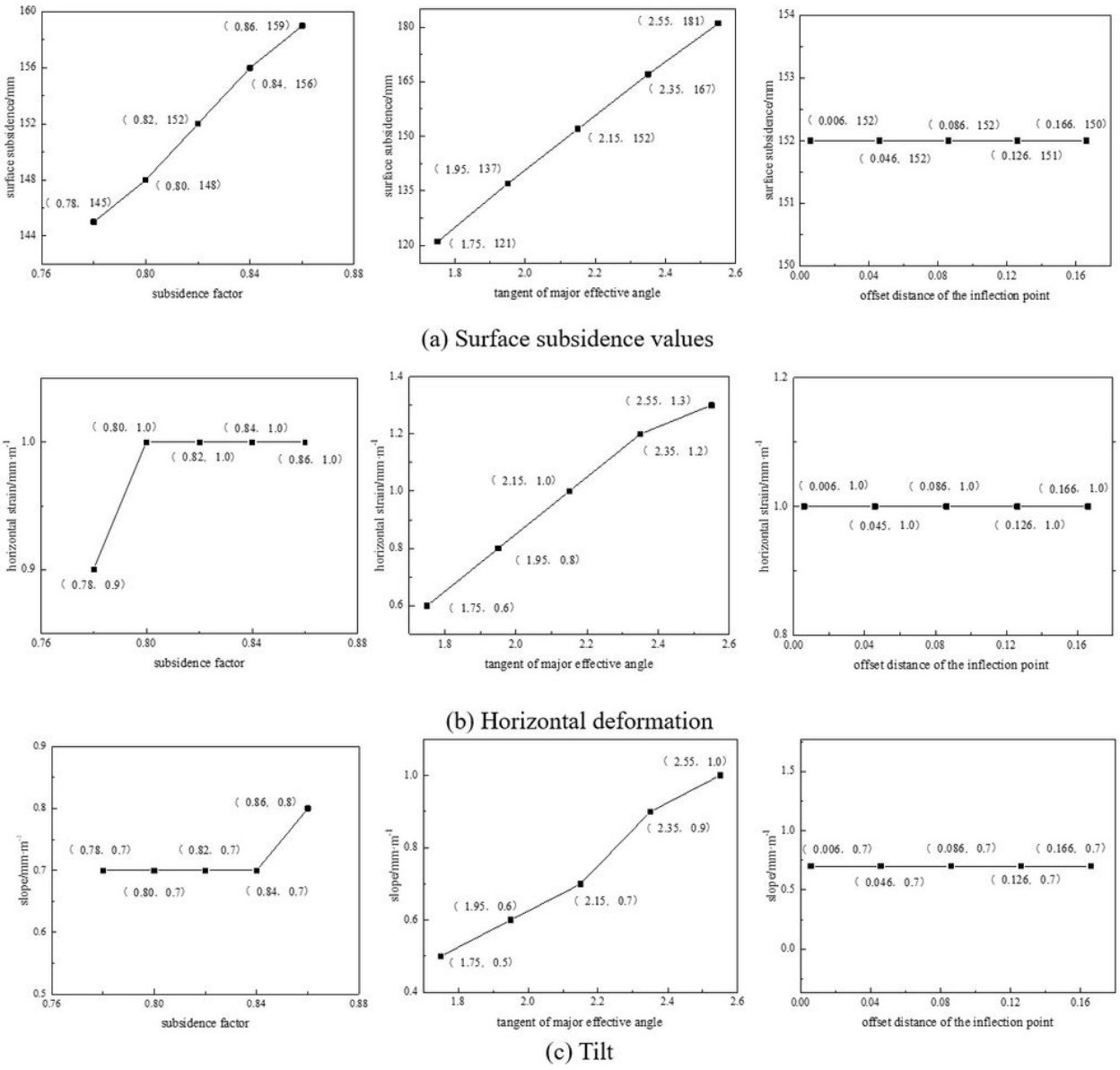


## Figure 12

Predicted results